Conducting Layered Materials

DOI: 10.1002/ange.201104050

$Rb_4Sn_5P_4Se_{20}$: A Semimetallic Selenophosphate**

*In Chung, Kanishka Biswas, Jung-Hwan Song, John Androulakis, Konstantinos Chondroudis, Konstantinos M. Paraskevopoulos, Arthur J. Freeman, and Mercouri G. Kanatzidis**

Chalcophosphates are ternary (A/P/Q) and quaternary (A/M/P/Q) compounds with $[P_yQ_z]^{n-}$ anions in their structure, where M is a metal, A is an alkali metal, and Q is sulfur,[1] selenium,[2] or tellurium.[3] They can exhibit fundamentally and technologically important nonlinear optical[4] and ferroelectric properties,[5] reversible redox chemistry relevant to secondary batteries,[6] photoluminescence,[7] and phase-change properties.[8] However, no metallic selenophosphates have been reported to date. This lack is in striking contrast to the oxophosphate counterparts, which are a well-defined series of unusual metals, such as $(PO_2)_4(WO_3)_{2m}$, $A_x(PO_2)_4(WO_3)_{2m}$ (A = Na, K), and $A_x(P_2O_4)_2(WO_3)_{2m}$ (A = K, Rb, Tl, Ba).[9] The metallic properties of these phosphates derive from mixed valency of the transition metals. There have been attempts to explore chalcophosphate compounds as thermoelectric materials. For example, in light of the known alkali chalcophosphate compounds, the Tl^+ analogues $Tl_3Ti_2P_5S_{18}$, $Tl_2CeP_2S_7$, $TlTiPS_5$, and $Tl_2BiP_2S_7$ were investigated.[10] However, they were wide-gap semiconductors and too resistive for such applications. Inclusion of a transition metal gave a better-conducting semiconductor $Ni_3Cr_2P_2Q_9$ (Q = S, Se).[11]

Herein, we report on $Rb_4Sn_5P_4Se_{20}$, the first metallic selenophosphate. Its structure belongs to a class not previously known for this family, namely, a lamellar hybrid of "conducting" $[Sn_5Se_8]$ layers and "insulating" $[P_2Se_6]$ ligands. The structure is unique in that the $[P_2Se_6]^{4-}$ anions coordinate solely to the outer shell of the $[Sn_5Se_8]$ backbone layers. Consequently, the core of the latter consists only of Sn–Se bonds and is free of $[P_ySe_z]^{n-}$ units. Temperature-dependent electrical conductivity, thermopower, and Hall effect measurements on $Rb_4Sn_5P_4Se_{20}$ show n-type metallic behavior. The Pauli paramagnetic properties of $Rb_4Sn_5P_4Se_{20}$ are consistent with the metallic characteristics. The results of ab initio density functional theory (DFT) calculations using the all-electron full-potential linearized augmented plane wave (FLAPW) method[12] reveal that the metallic behavior originates from the overlap of conduction and valence bands and not any formal mixed valency.

$Rb_4Sn_5P_4Se_{20}$ was synthesized by the reaction of Sn/Rb_2Se/P_2Se_5/Se in a 1:1:1:5 molar ratio at 490 °C for four days. However, the complicated Lewis acid–base equilibria in the flux also yielded $Rb_3Sn(PSe_5)(P_2Se_6)$[13] as by-product. On the other hand, the direct combination of the elements and reaction at 515 °C gave SnP_2Se_6.[14] We could obtain pure $Rb_4Sn_5P_4Se_{20}$ only by direct combination reactions of Sn/Rb_2Se/P/Se at 850 °C. According to differential thermal analysis (DTA), $Rb_4Sn_5P_4Se_{20}$ melts congruently at 517 °C, and the melt crystallizes at 494 °C. The X-ray powder diffraction patterns before and after melting and recrystallization were identical (Supporting Information Figure S1).

$Rb_4Sn_5P_4Se_{20}$ crystallizes in the trigonal space group $P\bar{3}m1$.[15] The structure features thick anionic $[Sn_5P_4Se_{20}]_n^{4n-}$ layers (Figure 1 and Figure S2 in the Supporting Information).

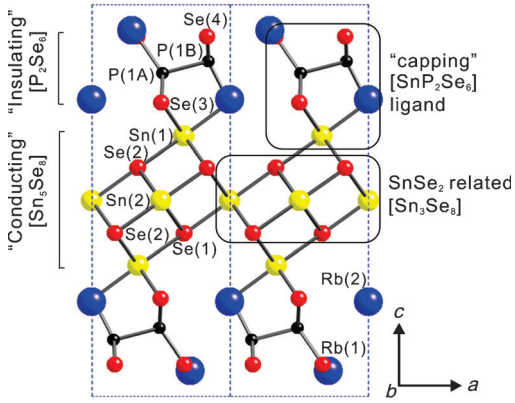

Figure 1. Structure of $Rb_4Sn_5P_4Se_{20}$ viewed down the *b* axis. All atoms are labeled. Disordered atoms are omitted for clarity. Rb blue, Sn yellow, P black, Se red.

tion). The layer is based on the $SnSe_2$ structure (CdI_2 type); the latter consists of planes of hexagonally packed Se atoms interleaved with planes of octahedral Sn atoms.[16] The removal of $^1/_4$ of the Sn^{IV} ions from the parent $SnSe_2$ layer creates vacancies and yields a $[Sn_3Se_8]^{4-}$ layer in $Rb_4Sn_5P_4Se_{20}$ (Figure 2). A more descriptive formula is $Rb_4[Sn^{IV}{}_3Se_8][Sn^{IV}(P_2Se_6)]_2$. The Sn vacancies created in the $SnSe_2$ layer are ordered and create a 2×2 supercell. That is, the values of the crystallographic *a* and *b* axes of 7.6163(4) Å are double those of $SnSe_2$ itself ($a = b = 3.811(2)$ Å).[16] The structure is com-

[*] Dr. I. Chung, Dr. K. Biswas, Dr. J. Androulakis, Prof. M. G. Kanatzidis
Department of Chemistry, Northwestern University
2145 Sheridan Rd. Evanston, IL 60208 (USA)
E-mail: m-kanatzidis@northwestern.edu
Homepage: http://chemgroups.northwestern.edu/kanatzidis/
Dr. J.-H. Song, Prof. A. J. Freeman
Department of Physics and Astronomy, Northwestern University
2145 Sheridan Rd. Evanston, IL 60208 (USA)
Dr. K. Chondroudis
Department of Chemistry, Michigan State University
East Lansing, MI 48824 (USA)
Prof. K. M. Paraskevopoulos
Department of Physics, Aristotle University of Thessaloniki
54124 Thessaloniki (Greece)

[**] Financial support was provided by the National Science Foundation (Grant DMR-1104965).

Supporting information for this article is available on the WWW under http://dx.doi.org/10.1002/anie.201104050.

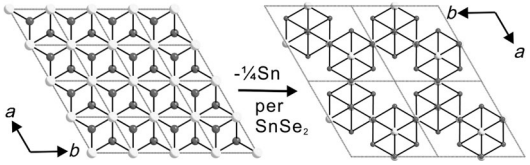

Figure 2. Formally underlying single $SnSe_2$ (left) and Sn_3Se_8 layers in $Rb_4Sn_5P_4Se_{20}$ (right) viewed down the *c* axis. Removal of one-quarter of the Sn^{IV} ions results in the defect Sn_3Se_8 layer. The unit cell is outlined with dashed lines. Sn white, Se gray.

pleted by "capping" of the $[Sn_3Se_8]$ layer by two $[SnP_2Se_6]$ fragments from opposite sides in an alternating arrangement. The SnP_2Se_6 fragments are located at the Sn vacancy points of the Sn_3Se_8 layers (Figure 1).

The two crystallographically unique Sn atoms are stabilized in a regular octahedral geometry. The Sn(1) atoms bond to three Se(3) atoms of the tridentate $[P_2Se_6]^{4-}$ anions and three neighboring Se(2) atoms of the $[Sn_3Se_8]^{4-}$ slabs (Figure 1), consequently connecting $[Sn_3Se_8]^{4-}$ and $[SnP_2Se_6]$ units to form anionic $[Sn_5P_4Se_{20}]_n^{4n-}$ layers. The Sn(2) atoms coordinate to two Se(1) and four Se(2) atoms to form the $[Sn_3Se_8]$ units. The Sn–Se separations are Sn(1)–Se(2) 2.6992(8) Å, Sn(2)–Se(1) 2.7119(6) Å, and Sn(2)–Se(2) 2.6972(5) Å, comparable to those found in $SnSe_2$ (2.682 Å). The $[Sn_5P_4Se_{20}]_n^{4n-}$ anionic layers are separated by two crystallographically independent Rb^+ cations; the Rb(1) and Rb(2) atoms are coordinated by twelve and eight Se atoms, respectively. The Rb–Se distances of the former range from 3.20(2) to 3.47(1) Å and those for the latter from 3.337(8) to 3.55(2) Å.

The $[P_2Se_6]^{4-}$ anions reside on the fixed-symmetry elements that they do not possess, that is, on the special position of the $P\bar{3}m1$ space group: (1/3, 2/3, *z*), Wyckoff position 2*d*, site symmetry 3*m*. They adopt three different orientations by positional disorder, and therefore, P atoms are one-third occupied (Figure S3 in the Supporting Information). A similar symmetry-related disorder is found in $Cs_{10}P_8Se_{20}$,[17] $K_{10}Sn_3(P_2Se_6)_4$,[18] and $[Mo_2Cl_8]^{n-}$.[19] Selected area electron diffraction patterns obtained by transmission electron microscopy and investigation of the reciprocal lattice using extended X-ray exposure did not reveal any superstructure or twinning (Figure S4 in the Supporting Information). We further confirm the correctness of crystal structure with disorder models by examining crystal structure in lower symmetry of the triclinic and monoclinic space group, for example, $P\bar{1}$ and *C*2/*m* (subgroup of $P\bar{3}m1$). We could still observe similar disorder behaviors, including positional disorder of the $[P_2Se_6]^{4-}$ units. Introducing additional available symmetry elements gave the space group $P\bar{3}m1$ from the space groups $P\bar{1}$ and *C*2/*m* and led to an improved R_1 value.

This unusual crystal structure derived from the defect layers of $SnSe_2$ and the black color of the crystals brought us to examine the temperature dependence of the charge-transport properties. For charge-transport measurements, we prepared large bubble- and crack-free polycrystalline ingots ca. 8–10 g) using the Bridgman technique (Figure 3a), and growth conditions were guided by the DTA results. The electrical conductivity decreases linearly with temperature

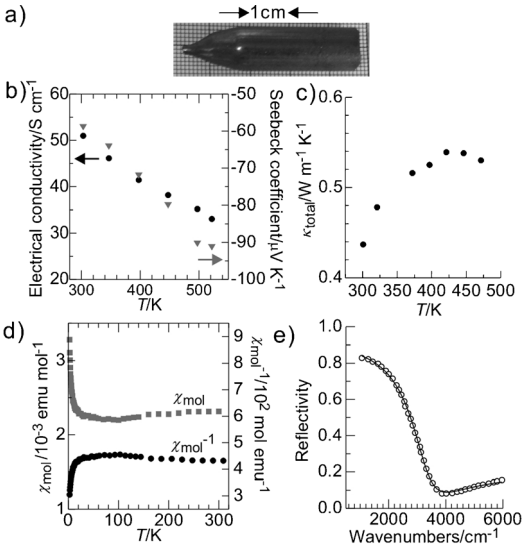

Figure 3. a) A representative ingot of $Rb_4Sn_5P_4Se_{20}$ grown in a Bridgman furnace. Temperature dependence of b) electrical conductivity (●) and Seebeck coefficient (▼) and c) total thermal conductivity κ_{total}. d) The magnetic susceptibility showing temperature-independent Pauli paramagnetic behavior. e) IR reflectivity spectrum of $Rb_4Sn_5P_4Se_{20}$ single crystal (○) and the best fit by the extended Drude model (black line).

over the entire temperature range, indicating metallic behavior (Figure 3b); the value at 300 K is 51 $S\,cm^{-1}$. The value measured on a small single crystal at 300 K is approximately 238 $S\,cm^{-1}$ (Figure S5 in the Supporting Information). The transport properties of chalcophosphate compounds typically reveal low conductivity. $Rb_4Sn_5P_4Se_{20}$ displays the highest electrical conductivity at room temperature, compared to other chalcophosphate materials such as $KNb_2P_2S_{12}$ (0.15 $S\,cm^{-1}$),[1d] $TlTiPS_5$ (ca. 6.7×10^{-5} $S\,cm^{-1}$),[10] $Ni_3Cr_2P_2Se_9$ (ca. 10 $S\,cm^{-1}$),[11] and $MnPS_3$ (ca. 10^{-8} $S\,cm^{-1}$).[20]

Thermoelectric power measurements gave negative Seebeck coefficients with linear dependence on temperature, suggesting n-type conduction; the value at 300 K is -59 $\mu V\,K^{-1}$. Seebeck coefficients measured on single crystals reflect the anisotropic crystal structure: -45 $\mu V\,K^{-1}$ along the $[Sn_5Se_8]$ layer parallel to the *ab* plane and -14 $\mu V\,K^{-1}$ perpendicular to it. Hall effect measurements show a phenomenological carrier concentration at room temperature of -1.66×10^{19} cm^{-3}, indicative of n-type conduction and consistent with the negative Seebeck coefficient. Note that this is the average value of conducting and insulating layers owing to the polycrystalline nature of the ingots.[21] The calculated mobility is 19.2 $cm^2\,V^{-1}\,s^{-1}$. In comparison, $SnSe_2$ is an n-type semiconductor with a lower electrical conductivity of 3.6 $S\,cm^{-1}$ and electron concentration of 10^{18} cm^{-3}.[22]

The total thermal conductivity κ_{total} as a function of temperature is extremely low value at 0.44 $W\,m^{-1}\,K^{-1}$ at room temperature (Figure 3c), which was measured perpendicular to the $[Sn_5P_4Se_{20}]_n^{4n-}$ layer using a vertically grown ingot. Such a low value might plausibly arise from the structural and compositional complexity of the compound; the presence of alkali metals that are loosely bound and likely mobile in the interlayer space likely scatters strong heat-carrying phonons.

The value of κ_{total} increases slightly with temperature, as observed previously in some metal chalcogenide thermoelectric materials containing alkali metals such as $A_{1+x}M_{4-2x}M'_{7+x}Se_{15}$ (A = K, Rb; M = Pb, Sn; M′ = Bi, Sb)[23] and $KBi_{6.33}S_{10}$.[24] The value of κ_{total} is the sum of the phonon (lattice vibrations) and electronic contribution. The electronic thermal conductivity κ_e was calculated using the Wiedemann–Franz law $\kappa_e = L\sigma T$, assuming the Lorentz number $L_o = 2.44 \times 10^{-8}\,W\,\Omega\,K^{-2}$. Then, the lattice conductivity κ_{lat} was calculated by subtracting the electronic component from κ_{total}. (Figure S6 in the Supporting Information). The result showed that κ_{total} is dominated by κ_{lat}. The heat capacity at room temperature is $0.19\,J\,g^{-1}\,K^{-1}$, and it increases with temperature monotonously (Figure S4 in the Supporting Information).

Molar magnetic susceptibility measurements of $Rb_4Sn_5P_4Se_{20}$ indicate temperature-independent, Pauli paramagnetic behavior (Figure 3d) consistent with metallic behavior. This observation is agreement with the charge-transport results. The "Curie tail" observed at low temperature often results from a trace of paramagnetic impurities in the sample. The data were corrected for ion core diamagnetism[25] of -1.13×10^{-3} emu mol^{-1} and were fitted to a modified Curie–Weiss law [Eq. (1)]:

$$\chi_m = \chi_0 + \frac{C}{T-\theta} \quad (1)$$

where χ_m is the molar susceptibility, χ_0 is the temperature-independent Pauli paramagnetic susceptibility, C is the Curie constant, and θ is the critical temperature. The best-fit parameters are $\chi_0 = 2.21 \times 10^{-3}$ emu mol^{-1}, $C = 2.41 \times 10^{-3}$ emu mol^{-1}, and $\theta = 0.41$ K. The value of the effective magnetic moment $\mu_{exp} = 0.43\,\mu_B$ was calculated from the C value of the fit, thus suggesting the formation of an itinerant spin system typical of metallic compounds.

Infrared reflectivity spectra were collected on single crystals in the 1000–6000 cm^{-1} spectral region at room temperature with a resolution of 2 cm^{-1} (Figure 3e). The minimum in reflectivity at approximately 3600 cm^{-1} is typical of a metallic system. The data were fitted by the equation of the extended Drude model for the complex dielectric function $\tilde{\varepsilon}$ [Eq. (2)]:[26]

$$\tilde{\varepsilon}(\omega) = \varepsilon_\infty \left[1 - \frac{\Omega_P^2 + i(\gamma_P - \gamma_0)\omega}{\omega(\omega - i\gamma_0)}\right] \quad (2)$$

Ω_P is the plasma frequency, γ_P the carrier damping constant at the frequency $\omega = \Omega_P$, γ_0 the damping value at $\omega = 0$, and ε_∞ the high-frequency permittivity. The application of this model fits well to the data with the fitting parameters of $\varepsilon_\infty = 7.1$, $\Omega_p = 3420$ cm^{-1}, $\gamma_p = 1154$ cm^{-1} and $\gamma_0 = 670$ cm^{-1}. The low value of ε_∞ is indicative of strongly damped phonon oscillations, consistent with the low thermal conductivity observed. The physical meaning of the double-damped Drude model is that the carrier damping is not constant but frequency-dependent [Eq. (3)]:[26]

$$\gamma(\omega) = \gamma_0 + (\gamma_P - \gamma_0)\frac{\omega^2}{\Omega_P^2} \quad (3)$$

The mobility μ_{opt} at $\omega = \Omega_P$, the DC optical conductivity $\sigma(0)$ at $\omega = 0$, and the free carrier's effective mass m^* were calculated to be $\mu_{opt} = 451$ cm^2 V^{-1} s^{-1}, $\sigma(0) = 2059\ \Omega^{-1}$ cm^{-1} and $m^*/m_0 = 0.018$ by the relations in Equations (4) and (5):

$$\mu_{opt} = \frac{e}{m^*\gamma_P}\sigma(0) = \frac{\varepsilon_\infty \Omega_P^2}{\gamma_0} \quad (4)$$

$$N = \Omega_P^2 m^* \varepsilon_\infty \quad (5)$$

The values of μ_{opt}, $\sigma(0)$, and N clearly establish that $Rb_4Sn_5P_4Se_{20}$ is semimetallic. The far-IR spectrum displays absorptions at 513, 488, 417, 301, and 213 cm^{-1}, which are characteristic of the $[P_2Se_6]^{4-}$ group.[27] Absorptions at 234 and 181 cm^{-1} account for Sn–Se vibrations.[28]

To understand the origin of the metallic and charge-transport properties, we performed electronic structure calculations using the highly precise full-potential linearized augmented plane wave (FLAPW) method[12] with the screened-exchange local density approximation (sX-LDA) as well as the Hedin–Lundqvist form of the exchange-correlation potential (LDA).[29] The sX-LDA method has been applied to a wide range of semiconductors and yielded excellent excited states owing to its better long-range treatment of the exchange-correlation hole compared to the LDA method.[3a,4b,30] Indeed, for $Rb_4Sn_5P_4Se_{20}$, the sX-LDA method reduces the significant LDA overlap (ca. 0.34 eV) between valence and conduction bands, resulting in semimetallic behavior (Figure 4a–c), which leads to small concentrations of electrons in the conduction band (along Γ–A), and holes in the valence band (near M). At nonzero temperatures, the L-point will also contribute to the hole-carrier population since the valence top at the L-point is only 0.01 eV lower than E_F. The low dispersions of the bands along the Γ–A direction

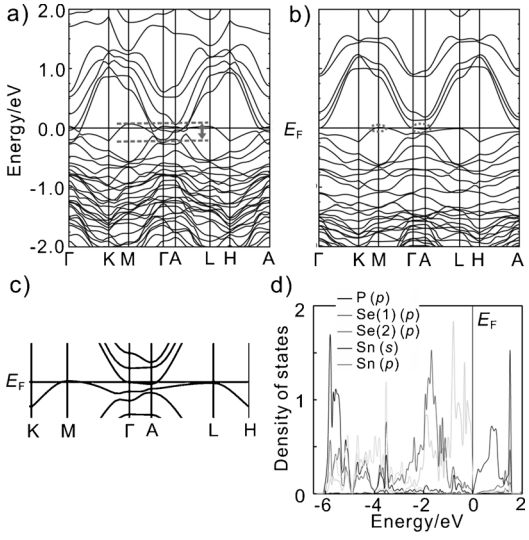

Figure 4. The calculated band structures of $Rb_4Sn_5P_4Se_{20}$ using a) the LDA method and b) the sX-LDA method. The overlap between the valence and conduction bands in (a) and the small electron and hole populations in (b) are indicated by dashed lines. c) The area involving the band overlap in (b), enlarged for clarity. d) The projected density of states for individual atoms calculated with the sX-LDA method.

originate from the two-dimensional characteristics of the structure. The n-type transport behavior discussed above suggests that the electrons are much more dominant in transport than the holes.

The angular-momentum-resolved density of states (DOS) for the different atom types in Figure 4d reveals that the low-energy states (−6 to −3 eV) are derived from the strong covalent interactions among P, Sn, and Se p orbitals. The predominant Se p orbitals in the higher-energy states (valence band maximum (VBM) ca. −3 eV) can be attributed to their lone-pair states. However, the strong ionic bonding between Se(2) and Rb atoms contributes exclusively to the valence-band top (−1 eV to VBM). The strong antibonding states between Sn s and Se p orbitals form a relatively strongly dispersed conduction-band bottom, which leads to the semimetal characteristics in the compound. At room temperature, it is envisioned that the transport properties are dominated by electrons of high mobilities, that is, the in-plane large dispersion of the bottom conduction bands.

The discovery of $Rb_4Sn_5P_4Se_{20}$ reflects the rich structural chemistry of Sn with $[P_yQ_z]^{n-}$ chalcophosphate ligands. The compound incorporates $SnSe_2$-derived building blocks with $[P_2Se_6]^{4-}$ ligands to form a unique low-dimensional structure. Its key element is the metallic character, which is attributed to the "conducting" $[Sn_5Se_8]$ layers. This behavior arises from overlap of conduction and valence bands in this formally valence-precise compound. In addition to the high electrical conductivity, $Rb_4Sn_5P_4Se_{20}$ shows extremely low thermal conductivity. This finding implies that a large family of chalcophosphate compounds could be developed for thermoelectric investigations, which have been so far excluded for such a purpose because of typical high resistivity. Investigation of new compounds with crystal structures related to $Rb_4Sn_5P_4Se_{20}$ would give more insight into how to circumvent such a problem.

Received: June 13, 2011
Published online: August 2, 2011

Keywords: conducting materials · density functional calculations · layered compounds · selenophosphates · thermoelectric properties

[1] a) M. G. Kanatzidis, *Curr. Opin. Solid State & Mater. Sci.* **1997**, *2*, 139–149; Mater. Sci. **1997**, 2, 139–149; b) Y. D. Wu, W. Bensch, *Inorg. Chem.* **2007**, *46*, 6170–6177; c) T. Komm, T. Schleid, *J. Solid State Chem.* **2005**, *178*, 454–463; d) C. Gieck, V, Derstroff, T. Block, C. Felser, G. Regelsky, O. Jepsen, V. Ksenofontov, P. Gütlich, H. Eckert, W. Tremel, *Chem. Eur. J.* **2004**, *10*, 382; e) C. Gieck, F. Rocker, V. Ksenofontov, P. Gutlich, W. Tremel, *Angew. Chem.* **2001**, *113*, 946–948; *Angew. Chem. Int. Ed.* **2001**, *40*, 908–911; f) J. Sayettat, L. M. Bull, J. C. P. Gabriel, S. Jobic, F. Camerel, A. M. Marie, M. Fourmigue, P. Batail, R. Brec, R. L. Inglebert, *Angew. Chem.* **1998**, *110*, 1773–1776; *Angew. Chem. Int. Ed.* **1998**, *37*, 1711–1714.

[2] a) C. Rotter, M. Schuster, S. Gebler, T. M. Klapotke, K. Karaghiosoff, *Inorg. Chem.* **2010**, *49*, 3937–3941; b) C. D. Morris, M. G. Kanatzidis, *Inorg. Chem.* **2010**, *49*, 9049–9054; c) A. Rothenberger, C. Morris, H. H. Wang, D. Y. Chung, M. G. Kanatzidis, *Inorg. Chem.* **2009**, *48*, 9036–9040; d) B. C. Chan, R. F. Hess, P. L. Feng, K. D. Abney, P. K. Dorhout, *Inorg. Chem.* **2005**, *44*, 2106–2113; e) K. Chondroudis. T. J. McCarthy, M. G. Kanatzidis, *Inorg. Chem.*, **1996**, *35*, 840–844.

[3] a) I. Chung, J. H. Song, M. G. Kim, C. D. Malliakas, A. L. Karst, A. J. Freeman, D. P. Weliky, M. G. Kanatzidis, *J. Am. Chem. Soc.* **2009**, *131*, 16303–16312; b) S. Jörgens, D. Johrendt, A. Mewis, *Chem. Eur. J.* **2003**, *9*, 2405–2410.

[4] a) I. Chung, J. I. Jang, C. D. Malliakas, J. B. Ketterson, M. G. Kanatzidis, *J. Am. Chem. Soc.* **2010**, *132*, 384–389; b) I. Chung, J. H. Song, J. I. Jang, A. J. Freeman, J. B. Ketterson, M. G. Kanatzidis, *J. Am. Chem. Soc.* **2009**, *131*, 2647–2656; c) I. Chung, J. I. Jang, M. A. Gave, D. P. Weliky, M. G. Kanatzidis, *Chem. Commun.* **2007**, 4998–5000; d) I. Chung, C. D. Malliakas, J. I. Jang, C. G. Canlas, D. P. Weliky, M. G. Kanatzidis, *J. Am. Chem. Soc.* **2007**, *129*, 14996–15006; e) P. G. Lacroix, R. Clement, K. Nakatani, J. Zyss, I. Ledoux, *Science* **1994**, *263*, 658–660.

[5] a) X. Bourdon, A. R. Grimmer, V. B. Cajipe, *Chem. Mater.* **1999**, *11*, 2680–2686; b) B. Scott, M. Pressprich, R. D. Willet, D. A. Cleary, *J. Solid State Chem.* **1992**, *96*, 294–300.

[6] a) Y. Kim, N. Arumugam, J. B. Goodenough, *Chem. Mater.* **2008**, *20*, 470–474; b) A. H. Thompson, M. S. Whittingham, US Pat., **1977**, *4049879*.

[7] a) S. Banerjee, J. M. Szarko, B. D. Yuhas, C. D. Malliakas, L. X. Chen, M. G. Kanatzidis, *J. Am. Chem. Soc.* **2010**, *132*, 5348–5350; b) Y. D. Wu, W. Bensch, *Inorg. Chem.* **2008**, *47*, 7523–7534; c) S. Banerjee, C. D. Malliakas, J. I. Jang, J. B. Ketterson, M. G. Kanatzidis, *J. Am. Chem. Soc.* **2008**, *130*, 12270–12272; d) G. Gauthier, S. Jobic, F. Boucher, P. Macaudiere, D. Huguenin, J. Rouxel, R. Brec, *Chem. Mater.* **1998**, *10*, 2341–2347.

[8] a) I. Chung, J. Do, C. G. Canlas, D. P. Weliky, M. G. Kanatzidis, *Inorg. Chem.* **2004**, *43*, 2762–2764; b) J. D. Breshears, M. G. Kanatzidis, *J. Am. Chem. Soc.* **2000**, *122*, 7839–7840.

[9] M. Greenblatt, *Acc. Chem. Res.* **1996**, *29*, 219–228.

[10] M. A. McGuire, T. K. Reynolds, F. J. DiSalvo, *Chem. Mater.* **2005**, *17*, 2875–2884.

[11] M. A. McGuire, F. J. DiSalvo, *Chem. Mater.* **2007**, *19*, 4600–4605.

[12] E. Wimmer, H. Krakauer, M. Weinert, A. J. Freeman, *Phys. Rev. B* **1981**, *24*, 864–875.

[13] K. Chondroudis, M. G. Kanatzidis, *J. Solid State Chem.* **1998**, *136*, 79–86.

[14] C. D. Carpentier, R. Nitsche, *Mater. Res. Bull.* **1974**, *9*, 1097–1100.

[15] Crystal data for $Rb_4Sn_5P_4Se_{20}$ at 173(2) K: Siemens SMART Platform CCD diffractometer, Mo Kα radiation ($\lambda = 0.71073$ Å), trigonal, $P\bar{3}m1$, $a = b = 7.6163(4)$, $c = 18.690(1)$ Å, $V = 938.91(9)$ Å^3, $Z = 1$; $M_r = 2638.41$ g mol^{-1}; $D_{calc} = 4.666$ g cm^{-3}, $D_{exp} = 4.64$ g cm^{-3}, $\mu = 27.989$ mm^{-1}, $2\theta_{max} = 56.56°$, 6157 total reflections, 952 unique reflections with $R_{int} = 4.17\%$, GOF = 1.137, 60 parameters, $R_1 = 3.40\%$, $wR_2 = 8.91\%$ for $I > 2\sigma(I)$, largest diff. peak and hole 1.264 and −2.391 e Å^{-3}. Further details of the crystal structure investigations may be obtained from the Fachinformationszentrum Karlsruhe, 76344 Eggenstein-Leopoldshafen, Germany (fax: (+49) 7247–808–666; e-mail: crysdata@fiz-karlsruhe.de) on quoting the deposition number CSD-422904.

[16] G. Busch, C. Fröhlich, F. Hulliger, E. Steigmeier, *Helv. Chim. Acta* **1961**, *34*, 359–368.

[17] I. Chung, D. Holmes, D. P. Weliky, M. G. Kanatzidis, *Inorg. Chem.* **2010**, *49*, 3092–3094.

[18] I. Chung, M. G. Kanatzidis, *Inorg. Chem.* **2011**, *50*, 412–414.

[19] F. A. Cotton, J. L. Eglin, *Inorg. Chim. Acta* **1992**, *198–200*, 13–22.

[20] P. A. Joy, S. Vasudevan, *J. Am. Chem. Soc.* **1992**, *114*, 7792–7801.

[21] C. M. Hurd, *The Hall effect in metals and alloys*, Plenum Press, New York, **1972**.

[22] G. Domingo, R. S. Itoga, C. Kannewurf, *Phys. Rev.* **1966**, *143*, 536 – 541.
[23] K. S. Choi, D. Y. Chung, A. Mrotzek, P. Brazis, C. R. Kannewurf, C. Uher, W. Chen, T. Hogan, M. G. Kanatzidis, *Chem. Mater.* **2001**, *13*, 756 – 764.
[24] M. G. Kanatzidis, T. J. McCarthy, T. A. Tanzer, L. H. Chen, L. Iordanidis, T. Hogan, C. R. Kannewurf, C. Uher, B. X. Chen, *Chem. Mater.* **1996**, *8*, 1465 – 1474.
[25] L. N. Mulay, *Magnetic susceptibility*, John Wiley & Sons, Inc., New York, **1963**.
[26] F. Gervais, in *Infrared and Millimeter Waves*, *Vol. 8* (Ed.: K. J. Button), Academic, New York, **1983**, p. 306.
[27] G. Kliche, *J. Solid State Chem.* **1984**, *51*, 118 – 126.
[28] J. Y. Harbec, S. Jandl, *Phys. Rev. B* **1982**, *25*, 6126 – 6129.
[29] L. Hedin, B. I. Lundqvist, *J. Phys. C* **1971**, *4*, 2064 – 2083.
[30] a) R. Asahi, W. Mannstadt, A. J. Freeman, *Phys. Rev. B* **1999**, *59*, 7486 – 7492; b) T. K. Bera, J. H. Song, A. J. Freeman, J. I. Jang, J. B. Ketterson, M. G. Kanatzidis, *Angew. Chem.* **2008**, *120*, 7946 – 7950; *Angew. Chem. Int. Ed.* **2008**, *47*, 7828 – 7832; c) J. H. Song, A. J. Freeman, T. K. Bera, I. Chung, M. G. Kanatzidis, *Phys. Rev. B* **2009**, *79*, 245203.